Elastic Response of Porous Matrix Plain Weave Fabric Composites: Part II—Results

J. L. KUHN AND P. G. CHARALAMBIDES
Department of Mechanical Engineering
The University of Maryland
1000 Hilltop Circle
Baltimore, MD 21228

(Received March 5, 1997)
(Revised August 26, 1997)

ABSTRACT: In this second of a two-part series of papers, the analytical and three-dimensional finite element models developed in Part I are implemented to predict the effective elastic response of both *stiff*-porous ceramic and *soft*-dense polymer matrix plain weave fabric composites. Analytical results obtained using a Modified Lamination Theory (MLT) model and which are based on four methods of unit-cell property averaging are presented. Effective elastic in-plane properties predicted via the finite element method for a single woven ply and for a laminate comprised of symmetrically arranged woven plies are also reported. Comparisons between the analytical estimates and the numerical predictions suggest that the Parallel (P-MLT) property averaging scheme yields, in an overall sense, good unit-cell effective property estimates. Thus, the P-MLT model was employed to conduct extensive parameter studies aiming at assessing the effects of the woven geometry and the overall microstructure on the effective elastic properties of *soft*- and *stiff*-matrix woven composites. *Soft*-matrix systems were shown to exhibit higher sensitivity to the unit-cell woven morphology and fiber/matrix elastic mismatch when compared to their *stiff*-matrix counterparts. On the other hand, the effective elastic properties of *stiff*-matrix systems were shown to be substantially reduced with increasing interbundle matrix porosity, and were also shown to be rather sensitive to the elastic properties of the thin fiber and bundle coatings. Surface contour data obtained from 3-D finite element analysis provide strong evidence of local micro-bending and stress concentrations within the unit cell. In both *soft*- and *stiff*-matrix systems, the out- of-plane normal and shear stresses along the bundle/matrix interface surfaces were shown to be at least an order of magnitude smaller than the predicted normal bundle stress along the fiber direction. This work presents detailed analytical and numerical parameter studies, and explores for the first time the relations between the microstructure and macromechanical woven composite response.

KEY WORDS: elastic, effective, properties, plain weave, composites, fiber, bundles, unit-cell, finite elements, *soft*-polymer matrix, *stiff*-ceramic matrix, porosity, coating, volume fraction, microstresses, microstrains.

0021-9983/98/16 1472–36 $10.00/0
© 1998 Technomic Publishing Co., Inc.

1. INTRODUCTION

IN THIS ARTICLE we report on analytical and three-dimensional (3-D) finite element results on the in-plane effective elastic properties of plain weave fabric composites comprised of an either *soft*-dense polymer matrix or of a *stiff* and porous ceramic matrix phase. These results were obtained with the aid of the analytical and numerical finite element models developed in Part I [1] where an extensive literature review on the subject is also presented. Thus, in this section, we shall present a brief synopsis of the models developed in Part I with emphasis placed on the model variables used in conducting the parameter studies reported herein.

1.1 The Unit-Cell Geometry

As discussed in Part I, an analytical approximate model that yields effective elastic property estimates for plain weave fabric composites has been developed. The model utilizes a new class of geometry shape functions which are used to define in a continuous manner the woven bundle morphology as well as the surrounding interbundle matrix domain within the reference unit-cell shown in Figure 1. The reference geometry shown in the above figure, is obtained as the basic unit-cell sub-structure of an otherwise continuous woven ply. In Part I, the geometry shown in Figure 1 was identified as the one that preserves full symmetry and thus microstructural repeatability such that, when loaded using the appropriate symmetry or antisymmetry conditions, the re-

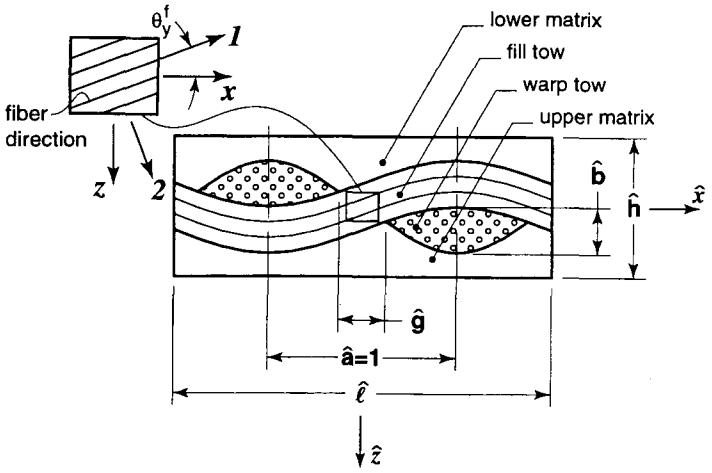

Figure 1. *Cross-sectional geometry and non-dimensional unit-cell parameters used in the development of the plain weave bi-directional undulation model (see Reference [1]).*

sponse of the unit-cell to the applied loading would represent the response of the continuum woven system subjected to the same loading. Conditions simulating single and multiple ply responses were established in Part I, and thus, associated results for single and multiple ply woven systems are reported herein.

As shown in Figure 1, the unit-cell geometry is defined with the aid of the following four independent geometry variables. The bundle waviness half period is defined using the parameter a. As discussed in Part I, the elastic response of the systems under consideration is studied in a non-dimensional environment such that the results could be applied to a general class of woven systems instead of a single specific system alone. Thus, all physical lengths were normalized with respect to a characteristic length which for the case under consideration was taken to be equal to the bundle undulation half period a and, as shown in Figure 1, the normalized bundle half period $\hat{a}$ is taken to be equal to unity. Henceforth, all other physical dimensions shall be normalized with respect to the reference length a. As shown in Figure 1, the reference unit-cell has a normalized length $\hat{l} = l/a$, and a normalized height $\hat{h} = h/a$. The fiber bundles which are also referred to as the tows are characterized using the maximum normalized height of their cross section $\hat{b} = b/a$, while the spacing between bundles is denoted by $\hat{g} = g/a$. Thus, as shown in Figure 1, the reference unit-cell is comprised of bundles woven in a plain weave orthogonal morphology. In the development of the unit-cell model in Part I, woven system terminology consistent with existing literature [7–21] was employed. Thus, the tows in the x global direction were referred to as the warp tows whereas their orthogonal tows aligned with the global y direction were referred to as the fill tows.

1.2 Model Microconstituents

The Modified Lamination Theory (MLT) model developed in Part I, treats the tows as a homogeneous orthotropic material with varying directional properties consistent with the undulating tow geometry. At this mesoscopic level of analysis, the surrounding interbundle matrix phase is treated as an effective linear elastic and isotropic medium. The above effective mesoscopic constituent property approach, has been the standard two-phase approach used in the literature in deriving model estimates for the overall effective elastic properties of the woven unit-cell. In the model developed in Part I, however, an additional level of analysis was added for the first time, aiming at incorporating in a consistent manner the effects of an intricate and often rather complex woven cell microstructure exhibited by Chemical Vapor Infiltration (CVI) ceramic matrix woven systems such as that shown in the micrographs in Figure 2 which were obtained by Zok et al. [2], Steyer and Zok [3], McNulty and Zok [4]. Thus, at this new level of microstructural analysis, the tows were considered to be comprised of several microconstituents whose effects on the mesoscopic tow response were accounted

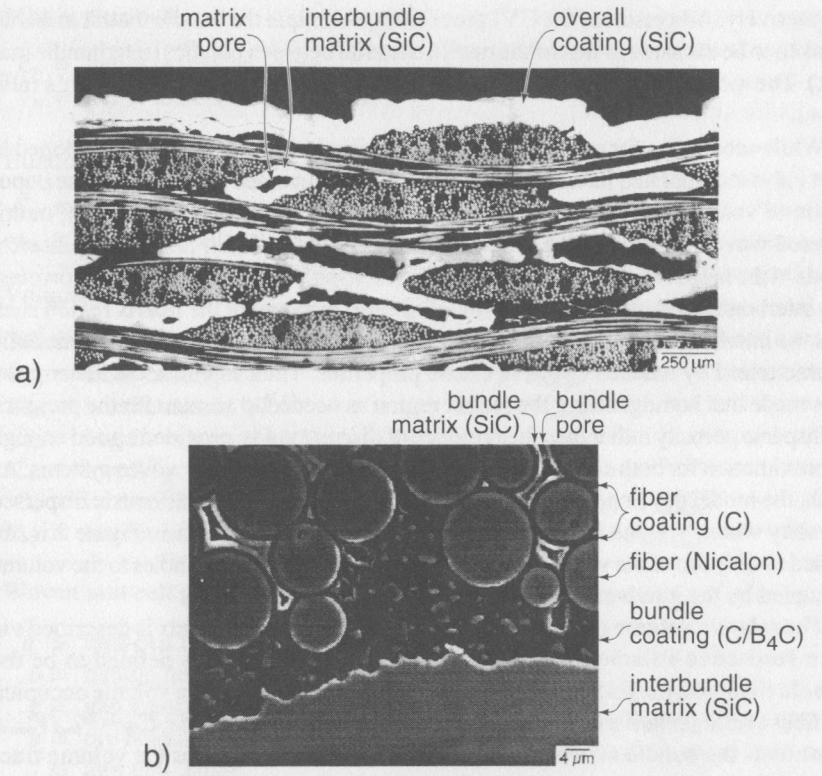

Figure 2. *Micrographs of a CVI ceramic matrix woven composite provided by Zok et al. [2]. (a) A composite laminate comprised of several randomly stacked woven plies. (b) An enlarged view of a region along the edge of a fiber bundle.*

for by employing various micromechanics models. More specifically, the orthotropic fiber reinforcements within the tows were considered to be coated by a relatively thin and elastically isotropic film. The bundle matrix was considered to be a porous medium simulating the bundle matrix porosity shown in Figure 2 which resulted during the CVI material processing. Finally, the bundle micromechanics also accounted for the presence of an overall elastically dissimilar bundle coating consistent with the experimental evidence shown in Figure 2.

The bundle fiber reinforcements were considered to be themselves linear elastic and orthotropic with the properties E_L^f, ν_L^f and G_L^f denoting the longitudinal fiber elastic modulus, Poisson's ratio, and shear modulus respectively, and E_T^f and ν_T^f denoting the transverse fiber modulus and Poisson's ratio respectively. The isotropic elastic modulus and Poisson's ratio of the fiber coating are denoted by E_{fc} and ν_{fc}, respectively, while those of the bundle coating are represented by E_{bc} and ν_{bc}

respectively. As a result of the CVI processing technique the bundle matrix material is taken to be the same as that of the matrix material between bundles (interbundle matrix). The modulus of the fully dense matrix is denoted by E_m and its Poisson's ratio by ν_m.

While accounting for a rather complex tow microstructure, the model developed in Part I also incorporated interbundle matrix porosity as needed to account for the population of voids in the matrix region between bundles. As discussed in Part I, multilayered woven systems of the type shown in Figure 2, exhibit rather large discrete voids in the matrix region between bundles. In *soft*-polymer matrix systems, however, the interbundle matrix porosity is often dispersed throughout the matrix region such that the interbundle matrix phase could be modeled using a homogenized elastic solid characterized by reduced effective elastic properties. Thus, in Part I, the assumption was made that homogenizing the matrix region as needed to account for the presence of disperse porosity rather than the presence of discrete voids, provided a good enough approximation for both *soft*-polymer and *stiff*-CVI ceramic matrix woven systems. As such, the model developed in Part I, does account for an interbundle matrix dispersed porosity whose volume fraction for systems similar to that shown in Figure 2 is obtained as the ratio of the volume occupied by the voids between bundles to the volume occupied by the interbundle matrix region.

The relative volume occupied by each of the above constituents is described via their respective volume fractions as follows: $C_f = V_f/V_{bundle}$ is defined to be the bundle fiber volume fraction, $C_{fc} = V_{fc}/V_{bundle}$ is used to denote the volume occupied by fiber coating relative to the total volume occupied by the bundle, $C_{bm} = V_{bm}/V_{bundle}$ represents the bundle matrix volume fraction, $C_{bc} = V_{bc}/V_{bundle}$ is the volume fraction of the bundle coating layer, and $C_{bp} = V_{bp}/V_{bundle}$ represents the void or porosity volume fraction within the bundle itself. In addition, the model incorporates as an independent variable, the interbundle matrix volume fraction defined as $C_m = V_{matrix}/(V_{total} - V_{bundles})$ and the volume fraction for the interbundle matrix voids or porosity which is defined as $C_{mp} = V_{voids}/(V_{total} - V_{bundles})$. Note that $C_f + C_{fc} + C_{bm} + C_{bp} + C_{bc} = 1$ and $C_m + C_{mp} = 1$. For the sake of clarity, the unit-cell microstructural parameters presented above are summarized as follows:

Fiber parameters

$E_L^f \equiv$ fiber longitudinal modulus
$E_T^f \equiv$ fiber transverse modulus
$\nu_L^f \equiv$ fiber longitudinal Poisson's ratio
$\nu_T^f \equiv$ fiber transverse Poisson's ratio
$G_L^f \equiv$ fiber longitudinal shear modulus

Fiber coating parameters

$E_{fc} \equiv$ fiber coating modulus
$\nu_{fc} \equiv$ fiber coating Poisson's ratio

Matrix parameters

$E_m \equiv$ dense matrix modulus
$\nu_m \equiv$ dense matrix Poisson's ratio

Bundle coating parameters

$E_{bc} \equiv$ bundle coating modulus
$\nu_{bc} \equiv$ bundle coating Poisson's ratio

Volume Fraction (VF)

$C_f \equiv$ fiber VF $\equiv V_f/V_{bundle}$
$C_{fc} \equiv$ fiber coating VF $\equiv V_{fc}/V_{bundle}$
$C_{bm} \equiv$ bundle matrix VF $\equiv V_{bm}/V_{bundle}$
$C_{bp} \equiv$ bundle microvoid VF $\equiv V_{bp}/V_{bundle}$
$C_{bc} \equiv$ bundle coating VF $\equiv V_{bc}/V_{bundle}$
$C_m \equiv$ interbundle matrix VF $\equiv V_{matrix}/(V_{total} - V_{bundles})$
$C_{mp} \equiv$ interbundle matrix microvoid VF $\equiv V_{voids}/(V_{total} - V_{bundles})$

Woven unit cell geometry

$a \equiv$ unit-cell half period
$b \equiv$ bundle height
$g \equiv$ gap width
$h \equiv$ ply height
$l \equiv$ unit cell length

1.3 Micromechanics Models and Constituent Homogenization

The complex bundle microstructure and porous interbundle phase described above were homogenized with the aid of appropriate micromechanics models to yield the effective mesoscopic properties of the homogenized tows and interbundle matrix which comprise the standard tow-matrix constituent woven composite. More specifically, the bundle homogenization was carried out in a hierarchical four-step homogenization process. During the first step, the properties of the fiber reinforcements and those of the fiber coating are combined via Hashin's Composite Cylinder Assemblage (CCA) model to obtain the effective properties of the homogenized fiber. During the second step, the porous solid model employed by Bassani [22] is used to obtain the effective properties of the porous bundle matrix. In the third step, Hashin's CCA model is used again to obtain the homogenized mesoscopic properties of the fiber bundle. During modeling step #4, Hashin's CCA model is employed once more as needed to evaluate the bundle coating effects on the effective elastic response of the homogenized bundle. In each fi-

ber/matrix homogenization step, the Hashin CCA model yields upper and lower bounds on the effective elastic properties. In general the upper and lower bounds were found to be relatively close. In this study the lower bound results from the Hashin model were used. The resulting mesoscopic properties after step #4 are used to obtain the macroscopic effective properties of the woven composite.

At the same time, the matrix phase was also homogenized using a dispersed porosity model employed by Bassani [22]. Clearly, in the case of CVI ceramic matrix systems, the above assumption can be used only as an approximation in estimating the effects of the presence of discrete large voids within the region between bundles. In light of this, a complementary study has been conducted as needed to assess the effects of the presence of such discrete large voids. The modeling and results of that study are presented elsewhere [23].

1.4 Woven Unit-Cell Effective Properties Model

As discussed earlier in this work, the in-plane effective elastic properties of the woven system were obtained analytically using a Modified Lamination Theory (MLT) model and numerically with the aid of a three-dimensional (3-D) finite element model. The effective mesoscopic properties of the woven tows and those of the interbundle matrix were used in conjunction with the new family of geometry shape functions developed in Part I as needed to establish the lamination morphology of elemental columns positioned at global coordinates (x, y) within the domain of the unit-cell. The mechanical response of each elemental column was then studied using the classical lamination theory. The laminate stiffnesses, obtained for each elemental column were then integrated across the unit-cell using one of four integration schemes as needed to establish the average woven unit-cell elastic response. These integration schemes are based on fundamental assumptions on the profile of the mid-plane strains and curvatures within the unit-cell under the application of external loads. For example, the Series or (S-MLT) integration scheme assumes that the force resultants remain constant across the length and width of the unit-cell. The Series-Parallel (SP-MLT) model, assumes that while the resultant forces remain independent of x, they may remain functions of y while their respective strains and curvatures exhibit a dependency on x and remain independent of y. The Parallel-Series (PS-MLT) integration scheme assumes the reverse of what is employed by the SP-MLT model. Finally the Parallel (P-MLT) model assumes that the unit-cell mid-plane strains and curvatures remain independent of position. Through the above process, the in-plane elastic effective properties of the woven system were obtained.

In this paper we report a wide range of results on the effective elastic properties of *stiff*-porous ceramic as well as *soft*-dense polymer matrix woven composites. In most instances, the analytical predictions are compared to numerical results which were obtained using the 3-D finite element pure tension and shear models presented in the companion paper, Part I, on modeling. Parameter studies are con-

ducted for both *stiff*- and *soft*-matrix systems as needed to highlight and explore the capabilities and limitations of the analytical and finite element models developed in the above mentioned studies. For comparison purposes with existing models [11–13], the *soft*-matrix results which are mostly associated with polymer matrix woven composites shall be presented and discussed next.

2. *SOFT*-MATRIX WOVEN COMPOSITE RESULTS

This group of results were obtained using mostly the material properties employed by Naik and Shembekar [3] who derived estimates of the effective elastic properties of a polymer matrix woven composite. In their case, a relatively *soft*-epoxy resin matrix was reinforced by a woven network of relatively stiff T-300 carbon fiber bundles. The longitudinal fiber elastic modulus was reported to be approximately equal to $E_L^f = 230\,\text{GPa}$ whereas the isotropic resin matrix modulus was $E_m = 0.0152 E_L^f = 3.5\,\text{GPa}$. In this work, the fibers within the tows are considered to be transversely isotropic with a longitudinal elastic and shear moduli E_L^f and G_L^f respectively, transverse elastic modulus E_T^f and major and minor Poisson's ratios ν_{LT}^f and ν_{TL}^f, respectively. The normalized elastic properties of the microconstituents used in this section of the study are shown in Table 1(a). In Table 1, all elastic and shear moduli are normalized with respect to the longitudinal fiber elastic modulus E_L^f Which, as discussed above for the Naik and Shembekar [13] system, was equal to approximately 230 GPa. The superscript l Indicates the lower bound from the Hashin model for the transversely isotropic tows. The subscript $\overline{m}$ indicates that the respective property is for that of the effective matrix.

As shown in Table 1(a), the bundle as well as interbundle matrix material is assumed to be linear elastic and isotropic with a normalized elastic modulus $\hat{E}_m = 0.0152$ and Poisson's ratio $\nu_m = 0.35$. The fiber volume fraction, which measures the relative volume occupied by the fibers within the fiber bundles alone, was taken to be $C_f = 0.74$. In this system, the matrix material both within the bundles as well as between bundles was considered to be fully dense and thus the matrix microporosity parameters C_{bp} and C_{mp} were set to be zero. In addition, for consistency with the approach taken by Naik and Shembekar [13], the fiber and bundle coating model micro-parameters were also taken to be zero. Thus, the remaining independent parameters involved in these *soft*-matrix woven system studies include the geometry parameters $\hat{a}$, $\hat{b}$, $\hat{g}$, $\hat{h}$ and $\hat{l}$ associated with the woven morphology as shown in Figure 1, the matrix/fiber moduli ratio $\lambda_{mf} = E_m/E_L^f$ *and the fiber volume fraction* C_f.

In the model implementation, auxiliary FORTRAN modules were developed as needed to calculate the bundle mesoscopic properties. These properties are calculated using the bundle micromechanics presented as part of the analytical modeling presented in Part I. For example, the bundle effective directional properties corresponding to the system microconstituents reported in Table 1(a) obtained via these auxiliary modules are those reported in Table 1(b). It is important to note that

Table 1. Non-dimensional input and output parameters for the soft-matrix system.

(a) *Soft*-Matrix—Input Parameters

T-300 Carbon Fiber	Epoxy Resin Matrix	Volume Fractions	Geometry
$\hat{E}_L = 1.0$	$\hat{E}_m = 0.0152$	$C_f = 0.74$	$\hat{a} = 1.0$
$\hat{E}_T = 0.174$	$\nu_m = 0.350$	$C_{bm} = 0.26$	$\hat{b} = 0.05$
$\hat{G}_L = 0.104$		$C_m = 1.0$	$\hat{q} = 0.0$
$\hat{G}_T = 0.0622$		$C_{mp} = 0.0$	$h = 0.1$
$\nu_L = 0.260$			$\hat{l} = 1.0$
$\nu_T = 0.399$			

(b) *Soft*-Matrix—Mesoscopic Output

Effective Tow	Effective Matrix	Overall Volume Fractions
$\hat{E}_{11} = 0.744$	$\hat{E}_{\overline{m}} = 0.0152$	$V_{fill} = 0.319$
$\hat{E}^{\ell}_{22} = 0.0631$	$\hat{G}_{\overline{m}} = 0.00564$	$V_{warp} = 0.319$
$\hat{G}_{12} = 0.0279$	$\hat{\nu}_{\overline{m}} = 0.350$	$V_{matrix} = 0.363$
$\hat{G}^{\ell}_{23} = 0.0217$		
$\hat{\nu}_{12} = 0.280$		
$\hat{\nu}^{\ell}_{23} = 0.384$		

(c) *Soft*-Matrix—Effective Unit-Cell Properties

Property	P-MLT	PS-MLT	S-MLT	SP-MLT	FEA Single	FEA Multiple
$\hat{E}_x$	0.249	0.247	0.119	0.150	0.194	0.250
$\hat{G}_{xy}$	0.0198	0.0191	0.0184	0.0191	0.0178	0.0178
$\hat{\nu}_{xy}$	0.0532	0.0700	0.0525	0.0541	0.264	0.0502

the mesoscopic elastic properties are needed as input data to the analytical MLT and the 3-D numerical finite element models. For the specific set of inputs outlined in Tables 1(a) and 1(b), each of the MLT and Finite Element models were used to compute the effective unit-cell properties, and the results are listed in Table 1(c). These results are included in Figure 3 and the corresponding discussion below applies directly to the data reported in the above table. Table 2 includes results from the Naik and Shembekar 2-D-WF [13] model as well as results obtained using the MLT and Finite Element models developed in Part I, all with matching input parameters. The geometry model used for the MLT and finite element models is different than that of the 2D-WF, and as such, slight differences are expected in the results. While the 2-D-WF and MLT results are in good agreement, distinct differ-

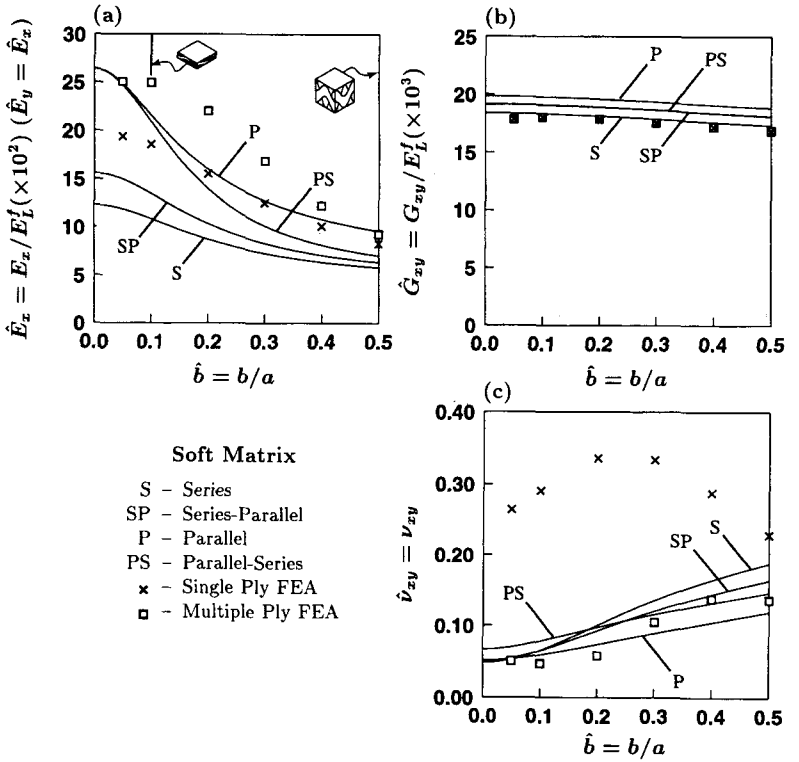

Figure 3. *The in-plane effective elastic moduli and Poisson's ratio for a soft-matrix woven composite with the bundle undulation ratio* b/a. *The results were obtained for a system with fiber volume fraction* $C_f = 0.74$, *bimaterial matrix/fiber moduli ratio* $E_m/E_L^f = 0.0152$, *and other unit-cell properties consistent with Table 1.*

ences exist between the finite element and analytical results. These discrepancies will be discussed in detail in the following paragraphs.

As discussed earlier, the effective properties of a woven composite system can be calculated analytically using the MLT approach in conjunction with the four integration/averaging schemes presented in Part I. These schemes are developed using fundamental assumptions on the distribution of the force and moment resultants as well as assumptions on the spatial dependency of the mid-plane strains and curvatures. For example, the Parallel-MLT [P-MLT, see Equation (34) in Part I] scheme assumes that the mid-plane strains and curvatures are constant through a given cross section in either the x or y direction. As such, the averaging force and displacement scheme reduces to the averaging of the spatially dependent laminate stiffnesses. On the other hand, the Parallel-Series-MLT [PS-MLT, see Equation

Table 2. Effective properties of a polymer matrix woven fabric composite predicted by the model of Naik and Shembekar [13] and the analytic and finite element models developed in Part I.

Effective Property	2-D WF [13] (PS)	MLT (PS)	2-D WF [13] (SP)	MLT (SP)	FE Single Ply	FE Multiple Plies
$\hat{E}_x$	0.249	0.247	0.155	0.150	0.194	0.250
$\hat{G}_{xy}$	0.0189	0.0191	0.0189	0.0191	0.0178	0.0178
$\hat{\nu}_{xy}$	0.076	0.070	0.061	0.054	0.26	0.050
Actual Properties for a Reference Modulus of E_L^f = 230 GPa						
E_x GPa	57.2	57.0	35.7	34.4	44.6	57.5
G_{xy} GPa	4.34	4.40	4.34	4.40	4.09	4.09
ν_{xy}	0.076	0.070	0.061	0.054	0.26	0.050

(37) in Part I] model assumes that the force and moment resultants are constant on the cross section which is perpendicular to the loading axis while its orthogonal cross section is subjected to constant mid-plane strains and curvatures. The Series-Parallel-MLT [SP-MLT, see Equation (36) in Part I] scheme is developed based on the reverse assumption from the PS-MLT scheme whereas the Series-MLT [S-MLT, see Equation (35) in Part I] scheme assumes constant force and moment resultants for any cross sections perpendicular to the x and y axis respectively.

The in-plane effective elastic properties estimated for *soft*-matrix woven composites obtained using the above mentioned averaging schemes are shown in Figure 3. The results presented in the figure were obtained using the woven constituent properties reported by Naik and Shembekar [13]. In addition to the analytical estimates which are represented by the solid lines, in Figure 3, finite element results obtained using a single woven layer model as well as results corresponding to the effective elastic response of a laminate comprised of a large number of symmetrically placed woven plies are also reported using the "x" and "□" symbols respectively. As shown in the figure, the in-plane effective elastic and shear moduli are normalized with respect to a reference modulus which for this study was taken to be equal to the longitudinal fiber modulus E_L^f. Thus, in Figure 3(a), the normalized effective modulus $\hat{E}_x = E_x/E_L^f$ is plotted against the relative bundle height to bundle wavelength ratio (see Figure 1) as measured through the non-dimensional bundle geometry parameter b/a.

It is important to note that while keeping the interbundle space g/a constant, the overall bundle volume fraction remains constant. At the same time the bundle cross-sectional shape and the orientation of the principal material directions within the bundles change as the aspect ratio b/a changes. For example, for a fixed interbundle space of $g/a = 0$ for the results shown in Figure 3, as the ratio b/a in-

creases the amplitude of the sinusoidal shape of the bundle cross sections and the out-of-plane rotation of the principal material directions of the fiber bundles increase. Because the overall tow volume fractions V_{fill} and V_{warp} and the fiber volume fraction C_f remain constant, it is expected that the actual shape of the bundle cross section will have a dramatically smaller effect on the results than the out-of-plane rotation of the fiber bundles.

The trends in the effective normalized shear modulus $\hat{G}_{xy} = G_{xy}/E_L^f$ and the in-plane major Poisson's ratio ν_{xy} with respect to the bundle geometry parameter b/a are shown in Figures 3(b) and 3(c) respectively. As in Figure 3(a), in the latter figures, the analytical estimates obtained using the four averaging methods discussed in Part I are represented by the solid lines and are labeled appropriately for each model, whereas the single and multiple ply finite element results are shown using the "x" and "□" symbols respectively.

As shown in the above figures, the analytical estimates obtained using the P-MLT, S-MLT, SP-MLT and PS-MLT models appear to fall within a relatively narrow bandwidth for the shear modulus shown in Figure 3(b), whereas they exhibit appreciable deviation from one another in predicting either the effective elastic modulus E_x and Poisson's ratio ν_{xy} shown in Figures 3(a) and 3(c) respectively. This apparent deviation between the predictions obtained using the four averaging schemes is shown to be greater for the effective elastic modulus E_x at low values of the geometry parameter b/a while diminishing with increasing b/a. On the other hand, in Figure 3(c), the reverse trend is shown to dominate the deviation between the analytical Poisson's ratio predictions obtained using the four averaging schemes with the largest deviation observed to be associated with relatively thick plies corresponding to $b/a = 0.5$.

The analytical results reported in Figure 3(a), with the exception of those corresponding to the P-MLT model, compare quite well with the results reported by Naik and Shembekar [13]. In making the comparison of the two sets of results, it is important to note that the ratio b/a used to plot the results in Figure 3 is equal to 1/2 h/a used to plot the results in Reference [13]. All input parameters except u/a are equal for each set of results, and $u/a = 0.6$ for the plot in Reference [13] while u/a is effectively equal to 1.0 for Figure 3(a). The dimension u is the distance between the flat regions of the fiber bundles measured in the plane of the unit-cell, and is not included in the current model. As u approaches 0 the geometry presented in Reference [13] approaches that of the earlier mosaic model of Ishikawa and Chou [7–12], and as u approaches 1 the geometry model of Reference [13] approaches the geometry shown in Figure 1 with some minor differences.

With the above in mind, it is clear that the P-MLT predictions reported in Figure 3(a) exhibit a downward trend with the ratio b/a whereas Naik and Shembekar's predict that the effective modulus E_x remains constant with b/a or h/a. The authors find this discrepancy somewhat puzzling in light of the observed agreement between the results obtained using the S-MLT, SP-MLT and PS-MLT averaging/in-

tegration models. While there are differences in the geometries as outlined above, their effects on the overall effective elastic response of the woven composite are expected to be minimal and could not explain the difference between the P-MLT results reported in Figure 3(a) and those reported in Reference [13].

It can be shown that the expression for the effective modulus resulting from the parallel averaging/integration scheme reduces to the simple rule of mixtures if $\theta_y^f = \theta_x^w = 0$ everywhere in the unit-cell and if the Poisson's ratios of each phase equal those of all other phases, and is given by

$$\hat{E}_x = V_{fill}\hat{E}_{11} + V_{warp}\hat{E}_{22} + V_{matrix}\hat{E}_{\bar{m}} \tag{1}$$

where V_{fill}, V_{warp}, and V_{matrix} are the overall volume fractions of the fill tow, warp tow, and interbundle effective matrix, respectively. The terms $\hat{E}_{11}$, $\hat{E}_{22}$, and $\hat{E}_{\bar{m}}$ are the longitudinal and transverse effective moduli of the tows and the effective modulus of the interbundle matrix, respectively.

The results can be expected to approach the rule of mixtures even for systems with mismatching Poisson's ratios. For the P-MLT model the above angles of orientation approach zero for $b/a \to 0$, and for the 2-D-WF model they approach zero for both $b/a \to 0$ and $u/a \to 0$. It can also be shown from Equations (1), (2), and (6) presented in Part I that the overall volume fractions of the current model are not a function of b. As a result, the overall volume fractions reported in Table 1 hold for $b/a \to 0$, and the resulting modulus computed using Equation (1) is $\hat{E}_x = 0.263$ as $b/a \to 0$ which is in very close agreement with Figure 3(a) as well as the respective plot in Reference [13].

The predicted downward trend in the normalized $\hat{E}_x$ with the aspect ratio b/a is intuitively consistent and can be explained as follows. As discussed above, the fiber bundles, at the mesoscopic level of modeling are considered to be elastically orthotropic with a longitudinal to transverse moduli ratio equal to E_{11}/E_{22}. In *soft*-polymer matrix composites, the stiffer and stronger fibers are used to reinforce the softer and often weaker matrix material. As a result, in such unidirectionally reinforced systems, the longitudinal modulus E_{11} which is dominated by the properties of the fiber reinforcements is often much higher than their transverse modulus E_{22} which is matrix dominated. In woven systems, the unidirectionally reinforced bundles themselves influence the overall effective properties of the woven composite consistent with the woven morphology. For example, in systems with small bundle undulations, i.e., small b/a ratios, the longitudinal bundle modulus E_{11} is expected to have a disproportionately larger influence on the unit-cell effective modulus $\hat{E}_x$ compared to the influence of the transverse bundle modulus E_{22}. However, as b/a increases, the bundle undulations also increase and thus, the relative influence of E_{22} on $\hat{E}_x$ should increase as well. Since, in *soft*-matrix systems E_{22} is much smaller than E_{11}, and as discussed above the influence of E_{22} on $\hat{E}_x$ in-

creases with b/a, it is consistent that the trends in $\hat{E}_x$ are shown in Figure 3(a) to decrease with b/a. As will be seen later on this study, this behavior is limited to *soft*-matrix systems and it does not apply to *stiff*-ceramic matrix woven composite, for their effective elastic response was found to be rather insensitive to the undulation ratio b/a.

As mentioned earlier in this section, single and multiple ply finite element results are also reported in Figure 3(a), 3(b), and 3(c) using the "x" and "□" symbols respectively. In Figure 3(a) it is shown that the single and multiple ply finite element predictions for the in-plane elastic modulus exhibit noticeable differences from one another for composites containing weaves with bundles of relatively large wavelength, i.e., $b/a < 0.1$. The single and multiple ply finite element predictions for the shear modulus shown in Figure 3(b) appear to be identical throughout the b/a ranges considered. The most dramatic difference however between the single layer versus a multiple ply laminate response appear to be associated with the effective Poisson's ratio predictions shown in Figure 3(c). At low b/a values, the Poisson's ratios predicted using a single layer finite element model are calculated to be in the range $0.25 \leq \nu_{xy} \leq 0.35$ whereas for the same b/a values the multiple ply laminate effective Poisson's ratio is calculated to be in the range $0.05 \leq \nu_{xy} \leq 0.08$. It is of interest to observe that the multiple ply finite element predictions for the in-plane Poisson's ratio are shown to be in better agreement with the analytical predictions when compared to the single ply results. This is not a surprising finding since the Modified Lamination Theory (MLT) approach used in the analytical model does not account for transverse interlaminar stresses and the associated out-of-plane twist which may be induced during uniaxial tension as a result of the woven microstructure. Clearly, in accordance with Figure 4(a), a *soft*-matrix single ply woven system may experience appreciable out-of-pane twist during remote tension whereas the lateral constraints associated with a multiple ply symmetric laminate, which is better represented by the analytical modeling assumptions used in Part I, do not allow for such twisting to take place [see Figure 4(b)]. Based on the comparison between the analytical predictions and the multiple ply laminate results it also appears that the Parallel-MLT model is, in an overall sense, in closer agreement with the 3-D finite element results. Thus, henceforth we shall use the Parallel-MLT model in obtaining further analytical estimates of the in-plane elastic effective properties of *soft*-matrix woven composites.

The trends in the normalized in-plane elastic modulus $\hat{E}_x$, shear modulus $\hat{G}_{xy}$ and Poisson's ratio ν_{xy} with the bundle geometry parameter b/a for systems of various interbundle space as measured by the normalized parameter g/a are shown in Figure 5. The solid lines represent analytical predictions obtained using the Parallel-MLT model whereas the "x" and "□" symbols represent finite element results which correspond to the top curve and the "+" and "◇" symbols represent finite element results which correspond to the bottom curve in each figure. As shown in the above figures, the top solid line corresponds to a system containing

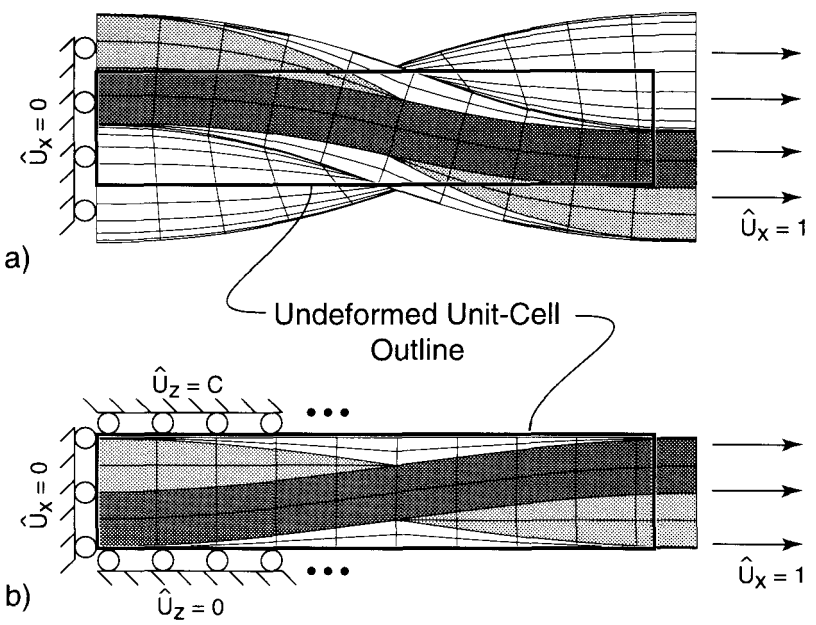

Figure 4. *The deformed mesh for a soft-matrix woven unit cell with* $\hat{b} = 0.1$. *(a) A single ply with traction free boundary conditions applied to the top and bottom faces. (b) A multiple ply system modeled with symmetry conditions applied to the top and bottom faces.*

no space between bundles, whereas the results represented by the bottom curves reflect the effective elastic response of systems with normalized distances equal to $g/a = 0.4$ between bundles. As before, it is important to note that at fixed b/a and C_f values, an increase in the space g/a between bundles refers to a new woven system whose bundles are narrower with fewer fibers and are placed further apart from one another. This is achievable by increasing the interbundle effective matrix material with increasing g/a while decreasing the bundle cross section. As a result the overall tow volume within the non-dimensionalized unit-cell is $\hat{V}_{tow} = \hat{V}_{fill} + \hat{V}_{warp} = 0.638$ for $g/a = 0$ [from Table 1(b)] and $\hat{V}_{tow} = 0.384$ for $g/a = 0.4$. In light of this, a constant fiber volume fraction C_f also implies that fewer fiber reinforcements are used overall.

As evident from Figure 5, rather good agreement is observed to exist between the analytical results obtained using the P-MLT model and the finite element multiple woven layer system predictions. As expected, the in-plane effective elastic stiffness and shear moduli for the woven systems under consideration reduce with increasing g/a and increasing b/a while an increase in the effective Poisson's ratio is predicted as shown in Figure 5(c). The analytical results for $\hat{E}_x$ are shown to be in better agreement with the multiple ply finite element results ("□" and "◇" sym-

bols) at low and high b/a values. As shown by the schematic in Figure 5(a), low b/a values correspond to rather thin section woven plies or laminates, whereas high b/a aspect ratio values correspond to fairly thick plies or laminates. For the latter systems, the basic assumption that the cross sections of the woven layer/laminate remain plane after deformation may be violated, which may explain the subtle but noticeable deviation of the analytical results from the 3-D finite element predictions as $b/a \rightarrow 0.5$. The effective shear modulus results shown in Figure 5(b), suggest that the analytical model predictions are slightly higher than those obtained from the 3-D finite element models. This is consistent with the results reported in Figure 3(b), where the P-MLT model is shown to predict higher effective shear moduli compared to the predictions obtained by the other three averaging schemes and the 3-D finite element model. As will be shown later in this section, shear

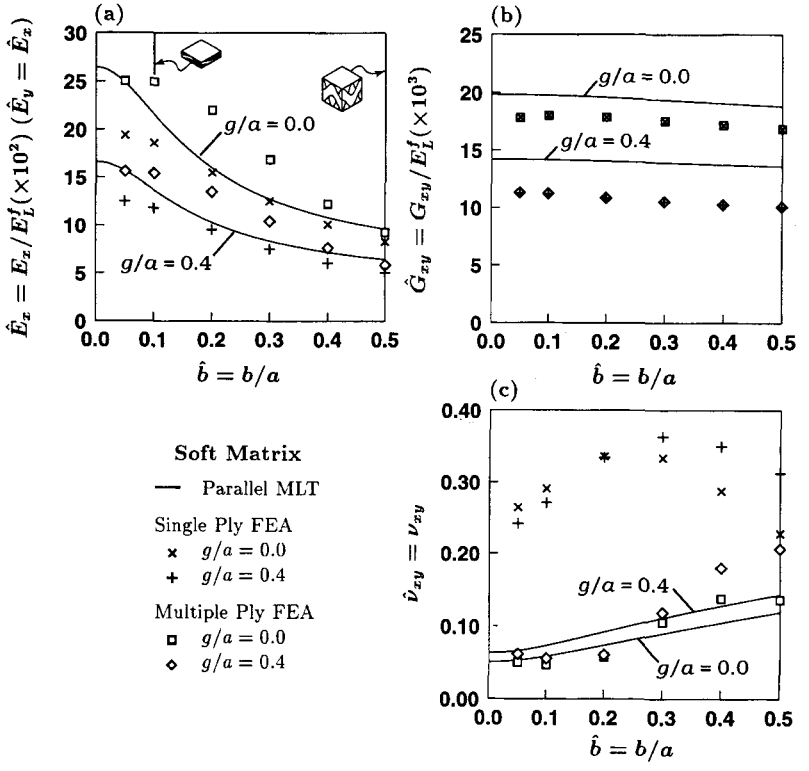

Figure 5. *The in-plane effective elastic properties for a soft-matrix woven composite with the bundle undulation ratio* b/a *for woven systems with bundle spacing equal to* g/a = *0.0 and 0.4. The results were obtained for a system with fiber volume fraction* C_f = *0.74, bimaterial matrix/fiber moduli ratio* E_m/E_L^f = *0.0152 (see Table 1).*

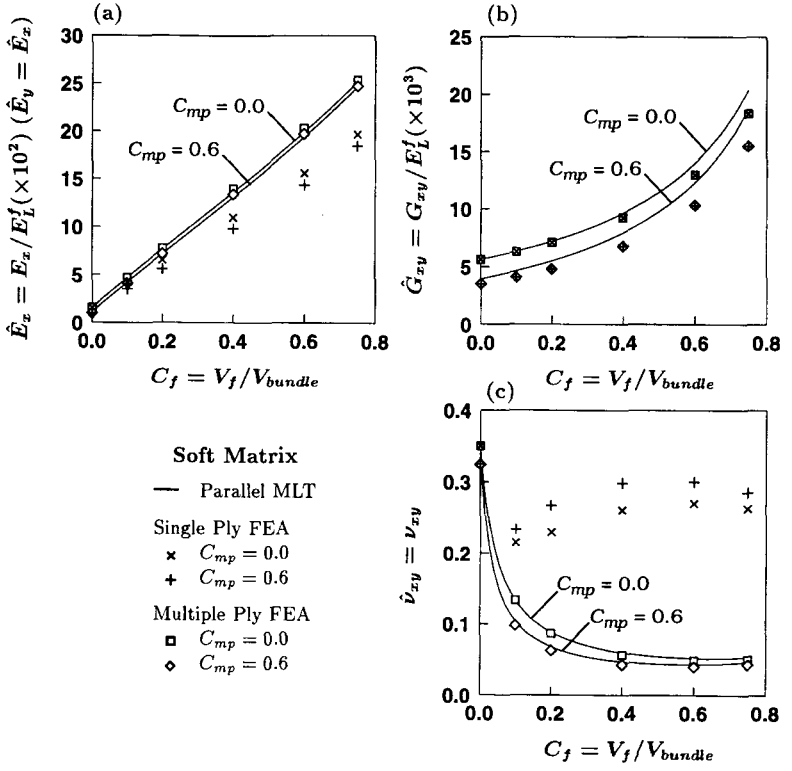

Figure 6. *The in-plane effective elastic properties for a soft-matrix woven composite against the bundle fiber volume fraction* C_f, *with interbundle matrix dispersed porosity density* C_{mp} = *0.6. (see Table 1 for remaining parameters.)*

modulus estimates which are in excellent agreement with the finite element results are predicted by the P-MLT and the other three averaging schemes when *stiff*-matrix woven composites are considered.

As discussed above, the results presented in Figures 3 and 5 were obtained under fixed fiber volume fraction C_f. In Figure 6, C_f, which is defined as the ratio between the volume occupied by the bundle fiber reinforcements to the volume of the bundle itself, is varied from 0 to 0.75 while keeping the fiber/matrix moduli ratio $E_L^f > E_m$ constant. Results corresponding to matrix porosity C_{mp} equal to 0.0 and 0.6 are presented. As expected, for a given combination of fiber and matrix materials as reflected through the choice of E_L^f and E_m such that $E_L^f > E_m$, and under fixed matrix porosity C_{mp}, the in-plane elastic moduli E_x and E_y increase with increasing bundle fiber volume fraction C_f. The analytical P-MLT predictions shown in Figure 6(a) appear to be in excellent agreement with the multiple ply 3-D finite ele-

ment results at all C_f values, and in good agreement with the laterally unconstrained single ply finite element results at low C_f values. Also at low C_f values, the analytical P-MLT in-plane effective shear modulus results G_{xy} shown in Figure 6(b) appear to be in excellent agreement with their numerical FE counterparts. As in Figure 3(b), the P-MLT shear modulus predictions are shown to be higher than the FE results. The results presented in Figure 3(b) also suggest that the deviation of the analytical and the 3-D FE results increase with increasing bundle fiber volume fraction C_f. In addition, the results reported in Figure 6(b), suggest that an overall non-linear dependency exists between the in-plane shear modulus G_{xy} and the bundle fiber volume fraction C_f.

The Poisson's ratio ν_{xy} trends with the bundle fiber volume fraction C_f are shown in Figure 6(c). The analytical P-MLT predictions are shown to be in remarkable agreement with the multiple ply 3-D FE results. Consistent with the results reported in Figure 3(c), the FE single ply estimates reported in Figure 6(c) appear to be substantially higher than both the analytical and 3-D multiple ply predictions. The numerical and analytical results shown for $C_f = 0.75$ and $C_{mp} = 0.0$ in Figure 6 correspond with the results plotted at $b/a = 0.05$ in Figure 3 (in which case $C_f = 0.74$). A strong correlation between the two sets of data is observed.

The dependency of the effective properties of the woven system on the elastic moduli ratio E_m/E_L^f for various degrees of fiber transverse anisotropy measured through the parameter E_T^f/E_L^f are shown in Figure 7. These results were obtained using a woven cell geometry consistent with that used in Reference [13]. Thus, in obtaining the above results, a bundle aspect ratio $b/a = 0.05$, a bundle fiber volume fraction $C_f = 0.74$, and an interbundle matrix porosity $C_{mp} = 0.0$ were used. The results shown in Figure 7 encompass both *soft*-matrix as well as *stiff*-matrix woven system responses. More specifically the trends in the woven effective elastic properties obtained for $E_m/E_L^f < 1.0$ correspond to the *soft*-matrix response whereas those obtained for $E_m/E_L^f > 1.0$ correspond to the *stiff*-matrix response. Here the terms *soft*-matrix and *stiff*-matrix are used in a general sense but they can often be used to represent *soft*-polymer and *stiff*-ceramic matrix woven composites respectively.

In accordance with the results reported in Figure 7(a), an overall agreement is shown to exist between the P-MLT analytical predictions and the 3-D single and multiple ply FE results. The comparison between the analytical and numerical results shown in the above figure indicate that there exists a better agreement between the two methods when predicting either the effective elastic modulus $\hat{E}_x$ [Figure 7(a)] or the shear modulus $\hat{G}_{xy}$ shown in Figure 7(b), when compared to the Poisson's ratio results reported in Figure 7(c). More specifically, the single ply FE Poisson's ratio predictions for *soft*-matrix systems, are shown to deviate from the multiple ply FE results and the results obtained analytically using the P-MLT model. This is consistent with earlier results reported in Figures 3, 5, and 6. However, as the ratio E_m/E_L^f becomes greater than unity, all in-plane effective elastic properties predicted either analytically

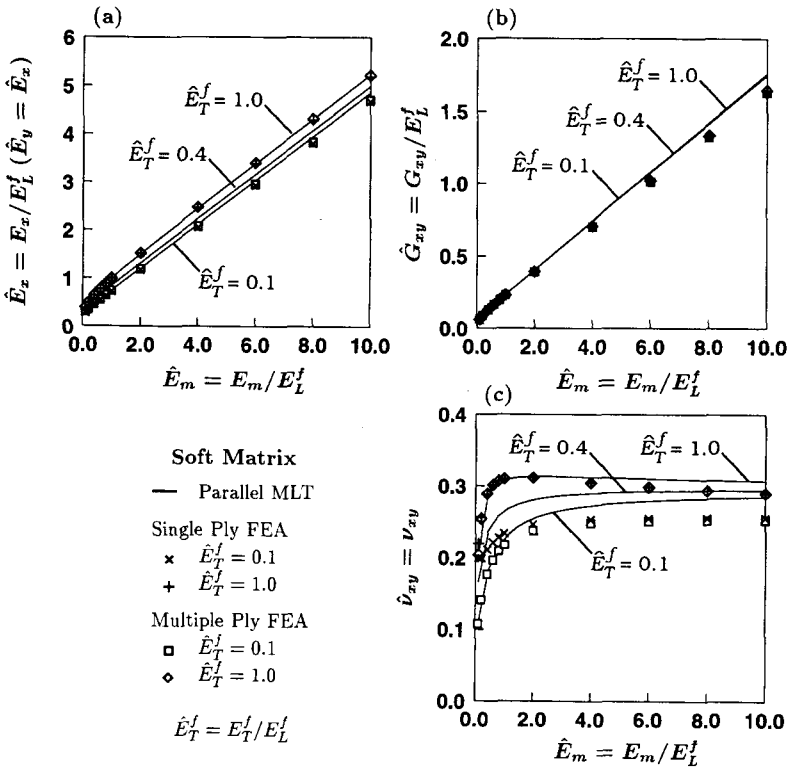

Figure 7. *The in-plane effective elastic properties for a soft-matrix woven composite with* E_T^f/E_L^f *equal to 0.1, 0.4, and 1.0, and remaining parameters given in Table 1.*

or numerically using the single or multiple ply 3-D FE models are shown to be in good agreement for the system under consideration. These trends reinforce further the selection of the P-MLT averaging analytical model as the one that best predicts the effective properties of *soft-* and *stiff*-matrix woven composites. It is of interest to observe that the transverse fiber modulus has a more pronounced effect on the elastic moduli E_x and E_y as well as on the major Poisson's ratio ν_{xy} but has little effect on the in-plane effective shear modulus G_{xy}.

3. *STIFF*-MATRIX WOVEN COMPOSITE RESULTS

Unlike the *soft*-matrix results presented above, which were mostly developed for comparison with results predicted by existing polymer matrix models, the *stiff*-matrix results are entirely new and can be used to interpret experimental data obtained using woven ceramic matrix composite test coupons. As discussed in the

modeling section of this work, several micromechanical constituent and woven geometry aspects have been incorporated into the effective properties models as needed to model more realistically the microstructure of woven CVI ceramic matrix composite such as the one shown in the micrographs provided by Zok et al. [2] in Figure 2.

Unlike the *soft*-matrix woven system studies, these studies assume that the fiber reinforcements within the longitudinal and transverse tows are homogeneous elastic and isotropic with an elastic modulus E_f and Poisson's ratio ν_f. In addition, in these studies the fibers are assumed to be coated by a thin elastic isotropic coating of modulus E_{fc} and Poisson's ratio ν_{fc}. The volume fraction of the fiber coating material is denoted by C_{fc}. The fully dense bundle and interbundle matrix material is characterized by a modulus E_m and Poisson's ratio ν_m. However, in this model (see Reference [1]), differential matrix porosities are allowed to exist in the matrix within the bundles and in the matrix between bundles whose densities are measured via the respective porosity volume fractions C_{bp} and C_{mp}. In addition, the *stiff*-matrix effective properties micromechanics model can also account for the presence of an altogether separate bundle coating phase whose isotropic elastic modulus is E_{bc} and Poisson's ratio ν_{bc} and its volume fraction is C_{bc}. Thus, the *stiff*-matrix results presented herein, when compared to those discussed for *soft*-matrix systems, include additional parameter studies as needed to elucidate the effects of bundle matrix porosity C_{bp}, interbundle matrix porosity C_{mp}, volume fraction of fiber coating C_{fc} and volume fraction of bundle coating C_{bc}. The *stiff*-matrix results are presented in Figures 8–11 and 15–17 and shall be discussed next.

As in the case of the *soft*-matrix studies, the results reported in the above mentioned figures were obtained through consistent non-dimensional studies using the analytical and 3-D finite element models discussed in the modeling part of this work (Part I). As indicated in Table 3(a), in these studies the reference elastic modulus is taken to be the isotropic fiber modulus E_f such that in the non-dimensional calculations $\hat{E}_f = 1.0$ was used. The non-dimensional properties for the fiber coating, dense matrix material and bundle coating are given in Table 3(a). In addition, in Table 3(a) various microconstituent volume fractions as well as the non-dimensional woven-cell geometry parameters used in these *stiff*-matrix studies are also given. The resulting mesoscopic properties for the "idealized" two-phase woven system indicating the bundle and interbundle matrix effective properties obtained through the bundle micromechanics and porous matrix models are shown in Table 3(b). It is important to note that these latter properties are the ones given as input in the 3-D finite element numerical studies. Results from the MLT and Finite Element models corresponding to the input of Tables 3(a) and 3(b) are listed in Table 3(c). In the above tables, the superscript l indicates the lower bound from the Hashin model for the transversely isotropic tows, which were selected for this analysis. The subscript $\overline{m}$ is used to denote ef-

Table 3. Non-dimensional input and output parameters for the stiff-matrix woven system.

(a) *Stiff*-Matrix—Input Parameters

Fiber	Fiber Coating	Matrix	Bundle Coating	Volume Fractions	Geometry
$\hat{E}_f = 1.0$	$\hat{E}_{fc} = 0.25$	$\hat{E}_m = 2.0$	$\hat{E}_{bc} = 0.5$	$C_f = 0.5$	$\hat{a} = 1.0$
$\nu_f = 0.2$	$\nu_{fc} = 0.25$	$\nu_m = 0.3$	$\nu_{bc} = 0.25$	$C_{fc} = 0.05$	$\hat{b} = 0.15$
				$C_{bm} = 0.1$	$\hat{g} = 0.15$
				$C_{bp} = 0.1$	$\hat{h} = 0.3$
				$C_{bc} = 0.25$	$\hat{l} = 1.0$
				$C_m = 0.7$	
				$C_{mp} = 0.3$	

(b) *Stiff*-Matrix—Mesoscopic Output

Effective Tow	Effective Matrix	Overall Volume Fractions
$\hat{E}_{11} = 0.737$	$\hat{E}_{\bar{m}} = 0.978$	$V_{fill} = 0.272$
$\hat{E}'_{22} = 0.656$	$\hat{G}_{\bar{m}} = 0.387$	$V_{warp} = 0.272$
$\hat{G}_{12} = 0.271$	$\hat{\nu}_{\bar{m}} = 0.264$	$V_{matrix} = 0.456$
$\hat{G}'_{23} = 0.264$		
$\hat{\nu}_{12} = 0.222$		
$\hat{\nu}'_{23} = 0.235$		

(c) *Stiff*-Matrix—Effective Unit-Cell Properties

Property	P-MLT	PS-MLT	S-MLT	SP-MLT	FEA Single	FEA Multiple
$\hat{E}_x$	0.824	0.820	0.817	0.820	0.823	0.823
$\hat{G}_{xy}$	0.324	0.323	0.321	0.322	0.322	0.322
$\hat{\nu}_{xy}$	0.239	0.238	0.237	0.238	0.237	0.237

fective matrix properties. Here we also note that in comparing Tables 1 and 3 the overall fiber volume fractions of the *soft*- and *stiff*-matrix systems are computed to be approximately 0.27 and 0.47, respectively.

In order to assess the effectiveness of the four analytical averaging schemes, i.e., the P-MLT, S-MLT, PS-MLT and SP-MLT models, the in-plane effective properties of *stiff*-matrix woven composites are plotted in Figure 8(a) against the aspect ratio b/a. As in the *soft*-matrix studies, in the same figure we also report numerical results obtained using the single and multiple ply 3-D finite element models. As shown in Figure 8, the analytical predictions obtained using the four averaging schemes mentioned above are found to be in excellent agreement with both

the single as well as the multiple ply FE results and appear to be rather insensitive to the aspect ratio b/a. The effect of the out-of-plane rotation will be most apparent for cases in which the longitudinal to transverse bundle effective modulus ratio $\hat{E}_{11}/\hat{E}_{22}$ is large. For the results shown in Figure 3, $\hat{E}_{11}/\hat{E}_{22} = 11.8$ while for the results shown in Figure 8, $\hat{E}_{11}/\hat{E}_{22} = 1.12$. The differences between these two cases show that the changes in the effective properties in Figure 3 are largely a result of the change in the bundle waviness.

While the results reported in Figure 8 correspond to a stiffer dense matrix woven system, i.e., $E_m = 2E_f$, the presence of the porosity [porosity densities are given in Table 3(a)] reduce the effective interbundle matrix modulus to a level comparable to that of the fiber modulus, i.e., $E_{\bar{m}} = 0.978E_f$ or even to that of the effective longi-

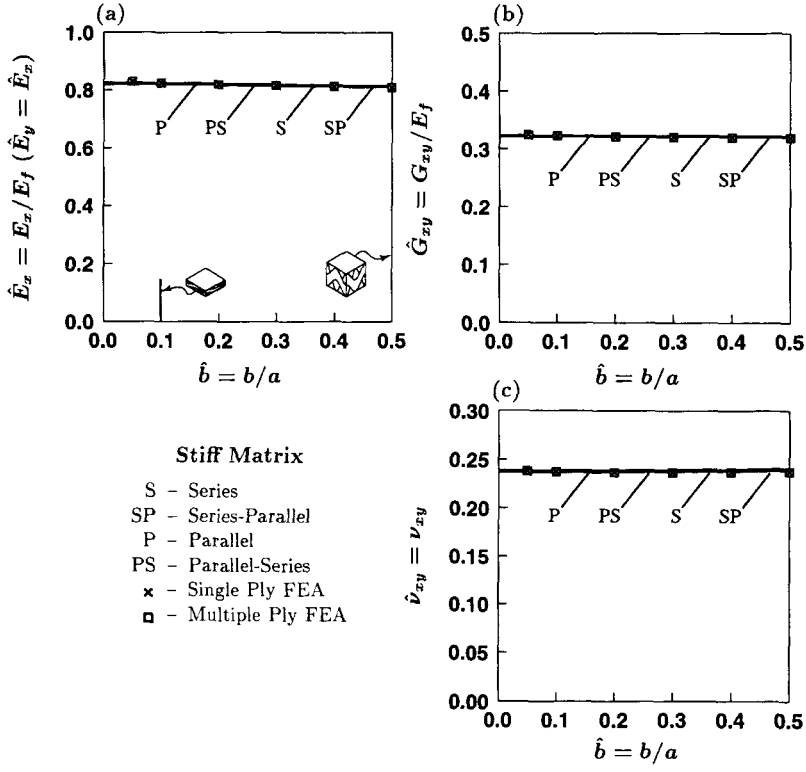

Figure 8. *The in-plane effective elastic properties versus woven bundle aspect ratio* b/a *for a stiff-matrix woven composite as predicted with the aid of the four stiffness integration schemes indicated above. All results were obtained for a system with fiber volume fraction* $C_f = 0.5$, *bimaterial matrix/fiber moduli ratio* $E_m/E_L^f = 2.0$, *and other unit-cell properties consistent with Table 3.*

tudinal bundle modulus which was calculated using bundle micromechanics to be $E_{11} = 0.737E_f$. As such one may argue that the agreement between the various model predictions reported in Figure 8 may to a large extent be due to the lack of strong material dissimilarity in the system under consideration. However, the results reported earlier in Figure 7, wherein an excellent agreement between the 3-D FE and analytical model predictions is also observed for strongly dissimilar fiber/matrix pairs, lessen the significance of this argument and further strengthen the conclusion made above regarding the effectiveness of the analytical models in predicting the effective elastic response of *stiff*-matrix woven composite comprised of complex microstructures.

In light of the above observations, we shall adopt the P-MLT averaging scheme model in obtaining further property estimates for *stiff*-matrix woven composites. Recall that the same P-MLT model was used in the *soft*-matrix parameter studies presented in the previous section. Thus, in Figure 9, P-MLT analytical effective property estimates are plotted along with 3-D FE results against the aspect ratio b/a. As indicated, the two curves included in each figure represent results obtained for woven systems with interbundle spacing g/a equal to 0.0 and 0.4. As before, the in-plane effective properties predicted for *stiff*-matrix woven systems, appear to be rather insensitive to the aspect ratio b/a. In addition, the P-MLT predictions are shown to be in excellent agreement with the 3-D FE results. At this point, it is worth stressing that the single and multiple ply FE results appear to be remarkably close to one another which is unlike the trends exhibited by the *soft*-matrix woven systems.

In Figure 10, a broad array of results aimed at assessing the effects of the bundle fiber volume fraction C_f, the fiber coating volume fraction C_{fc} and the bundle coating volume fraction C_{bc} on the in-plane effective elastic properties of *stiff*-matrix woven composites are presented. More specifically, the results in the left column of plots in the figure, were obtained by varying the bundle fiber volume fraction C_f while keeping the fiber and dense matrix material properties as well as the woven geometrical morphology fixed. As indicated in this column of plots, the sum $C_f + C_{bm} + C_{bp} = 0.7$ was also kept fixed while varying C_f as required to maintain an overall constant tow volume relative to the total volume occupied by the woven unit-cell. In order to isolate individual parameter effects, four curves of results each corresponding to a fixed bundle porosity C_{bp} are reported in Figure 10. For comparison purposes, 3-D single as well as multiple layer FE results corresponding to each of the analytical curves are also reported in the figure. As shown in the figure, the P-MLT analytical predictions are in remarkable agreement with the FE results. This strongly suggests that the analytical micromechanics models developed as part of this work and reported in the companion paper (Part I), can be used to accurately predict the effective elastic response of *stiff*-matrix woven systems comprised of complex microstructures.

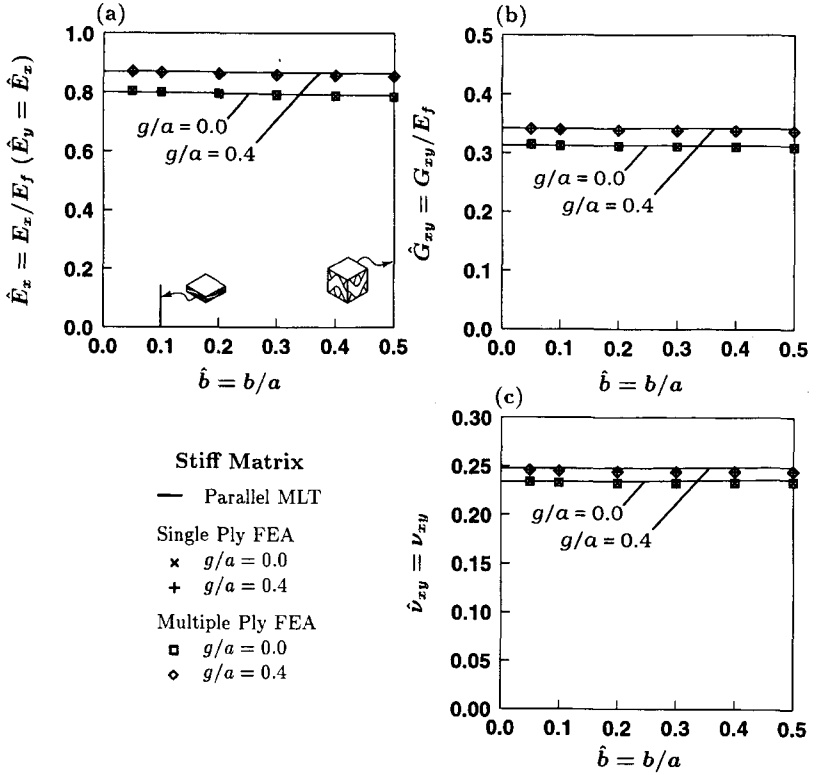

Figure 9. *The in-plane effective elastic properties versus woven bundle aspect ratio* b/a *for a stiff-matrix woven composite using the P-MLT stiffness integration model and parameters listed in Table 3.*

Since the bundle matrix porosity is kept constant along each curve in the left column of plots in Figure 10, and since the sum $C_f + C_{bm} + C_{bp} = 0.7$ is also fixed, it follows that for systems corresponding to the same curve the bundle fiber volume fraction is increased while decreasing the respective bundle matrix material. Thus, the allowable range for C_f decreases for results obtained at higher bundle matrix porosity C_{bp}. The above observation justifies the reason why the effective elastic property curves shown in each of the plots in Figure 10 are reported over a decreasing C_f range with increasing C_{bp} parameter values. Overall, the reported effective elastic properties exhibit a downward trend with increasing bundle fiber volume fraction C_f. This is an expected behavior since the addition of more relatively compliant bundle fibers should indeed result in an overall stiffness reduction of the woven *stiff*-matrix system. In contrast to the above results, an increase in the effective elastic

moduli with increasing C_f is predicted for *soft*-matrix composites as shown in Figures 6(a) and 6(b).

The results presented in the middle column of plots in Figure 10 show the influence of a thin fiber coating on the overall effective elastic response of *stiff*-matrix woven composites. In obtaining this set of plots, the sum $C_{fc} + C_{bm} + C_{bp} = 0.25$ was kept constant while varying the volume fraction of fiber coating C_{fc}. Each curve in the above set of data, also corresponds to a fixed value of the bundle matrix porosity parameter C_{bp}. Thus, the simulated increases in the volume fraction of fiber coating C_{fc}, which translates to an increase in the fiber coating thickness, takes place while decreasing the relatively stiffer bundle matrix material. For example, and in accordance with Table 3(a), these results were obtained using an elastically isotropic fiber coating of modulus E_{fc} =

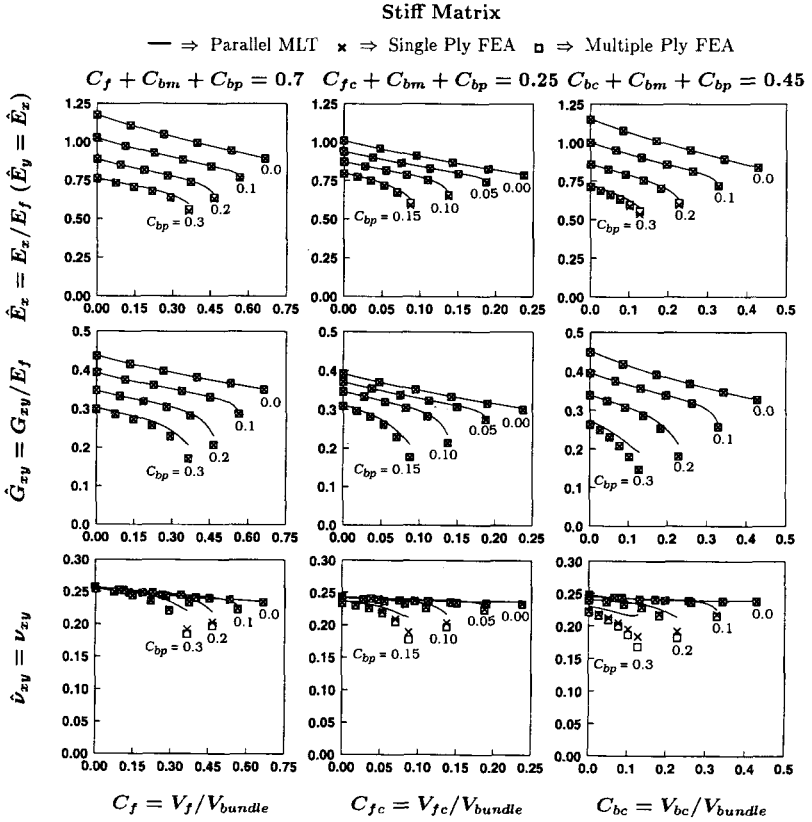

Figure 10. *The in-plane effective elastic properties for a* stiff*-matrix woven composite. The results are plotted against three woven bundle volume fractions (C_f, C_{bc}, and C_{fc}), and were obtained for a system with woven bundle aspect ratio b/a = 0.15, bimaterial matrix/fiber moduli ratio E_m/E_L^f = 2.0, and other unit-cell properties consistent with Table 3.*

$0.25E_f$ and Poisson's ratio $\nu_{fc} = 0.25$. As before, the addition of a more compliant fiber coating phase is predicted to yield a net reduction in the overall effective stiffness of the *stiff*-matrix woven system under consideration.

The results reported in the right column of plots in Figure 10 highlight the dependency of the in-plane effective properties of a *stiff*-matrix woven composite on the volume fraction of bundle coating C_{bc}. As discussed earlier elsewhere [1–6]. CVI ceramic matrix composites exhibit a rather complex microstructure. Among other aspects, the presence of a bundle coating has been identified by Zok et al. [2] and Bordia et al. [5,6] as an altogether separate microstructural entity. In this work and when compared with the other constituents, an elastically dissimilar bundle coating is incorporated into the bundle micromechanics such that the effective mesoscopic bundle properties are properly augmented to account for the bundle coating influence. In accordance with Table 3(a), the results reported in the right column of plots in Figure 10 have been obtained using bundle coating of isotropic elastic modulus $E_{bc} = 0.5E_f$ and Poisson's ratio $\nu_{bc} = 0.25$. Clearly, when $C_{bc} = 0$, the bundle coating thickness is zero which increases with increasing C_{bc}. Since, as indicated in Figure 10, this set of results was obtained keeping the sum $C_{bc} + C_{bm} + C_{bp} = 0.45$ constant, it is important to stress that at a constant bundle matrix porosity C_{bp}, the bundle coating thickness increase associated with the above set of results takes place by reducing the relatively stiffer bundle matrix volume fraction C_{bm}. As such, it is not surprising that the reported results also exhibit a downward trend with increasing C_{bc}.

In Figure 11, the in-plane effective elastic properties predicted analytically using the P-MLT model and numerically via 3-D finite element models are plotted against the dense matrix/fiber modulus ratio E_m/E_f. Various results reflective of the effects of the elasticity of the bundle coating are presented. Other than changing the matrix/fiber modulus ratio E_m/E_f along the horizontal axis, and the relative bundle coating modulus E_{bc}/E_f for each curve as denoted in Figure 11, the microstructural variables used in obtaining the above results are those given in Table 3(a). As shown in Figure 11 sightly lower effective in-plane elastic moduli are predicted for systems containing relatively soft bundle coatings, i.e., $E_{bc} = 0.2E_f$. At the same time, the in-plane effective elastic stiffnesses are shown to increase almost linearly with E_m/E_f. The influence of the ratio E_m/E_f on the Poisson's ratio however appears to be less pronounced, for, the predicted values appear to reach a plateau $E_m/E_f \rightarrow 10.0$. These results are consistent with those reported earlier in Figure 7 obtained under the *soft*-matrix woven system studies.

Overall, the results reported in Figures 8–11 are found to be in excellent agreement with their respective single and multiple layer 3-D finite element predictions. This, as discussed above, strongly suggests that the analytical micromechanics models developed as part of this work can be used to accurately predict the effective elastic response of *stiff*-matrix woven systems

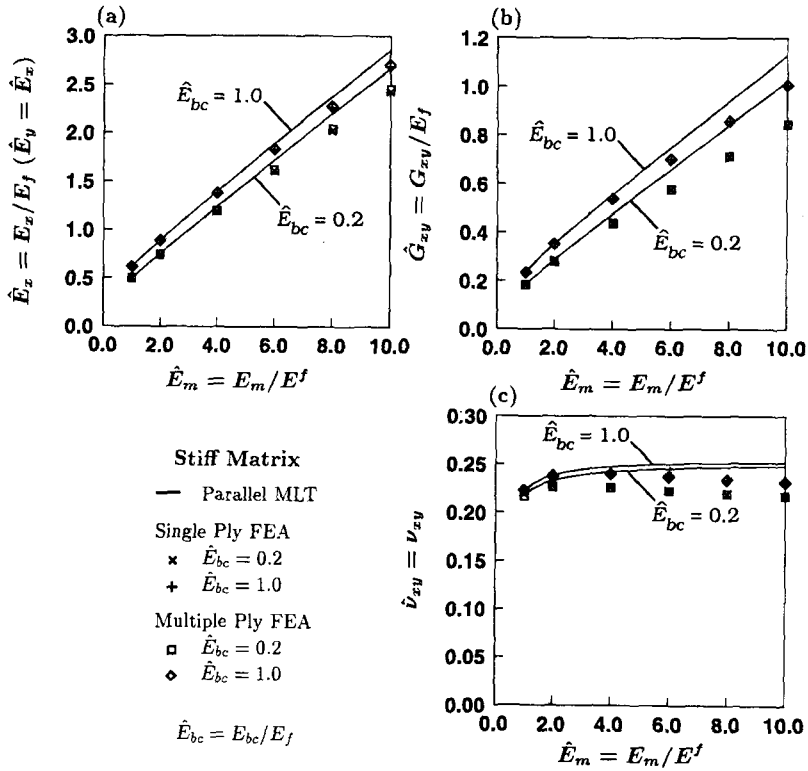

Figure 11. *The in-plane effective elastic properties for a* stiff-*matrix woven composite against matrix/fiber moduli ratio* E_m/E_L^f. *All results were obtained for system with unit-cell properties consistent with Table 3.*

comprised of complex microstructures. The trends reported in the above figure capture for the first time the influence of a rather complex microstructure on the effective elastic response of *stiff*-matrix woven composites such as the CVI ceramic matrix woven systems studied by Zok et al. [2], Steyer and Zok [3], McNulty and Zok [4], and Bordia et al. [5,6] and others. The results clearly suggest that mechanically distinct microstructural entities such as the fiber and bundle coatings, bundle matrix and interbundle matrix porosity and bundle fiber volume fraction may affect in a critical manner the effective elastic response of the woven composite. Thus, any attempt to minimize their influence and neglect their effects may lead to substantial errors in the interpretation of associated experimental data. At the same time, it is recognized by the authors that the results presented herein are encompassing only the elastic response of woven composites. In all likelihood, early on in their loading his-

tory, such microstructurally complex systems, may exhibit non-linearities induced by the evolution of several types of micro-damage such as matrix microcracking, bundle transverse cracking, bundle delamination, bundle cracking and macroscopic ply delamination and failure in woven ply composite laminates. In systems containing metal phases, plasticity may also play an important role in the overall mechanical response of the woven composites. While studies aiming at addressing some of the above non-linear phenomena and other complementary studies aiming at improving the models used to obtain the results reported herein are currently under way, the authors also feel that the models and results developed and presented in this two-part series of papers, i.e., Part I, and current paper, comprise the necessary first step for the development of a better understanding of the mechanical response of *soft*-polymer, *stiff*-ceramic and even metal matrix woven composites all of which may exhibit rather complex and distinctly different microstructures. The above discussion further highlights the need for interdisciplinary studies around the triad of material processing and specimen fabrication, mechanical and microstructural characterization, and analytical and numerical modeling. It is thus recommended that the models and results presented as part of this work, be used carefully in conjunction with the proper mechanical and microstructural characterization of *soft*-polymer and *stiff*-ceramic matrix woven systems as needed to interpret their possibly limited elastic response.

4. WOVEN UNIT-CELL MICROSTRAINS AND MICROSTRESSES

In their experiments, Zok et al. [2] reported microstrains, measured on the lateral free surface of a five woven ply CVI ceramic composite (see Figure 2), which were either substantially lower or higher than the applied macroscopic strain during uniaxial stretching. This result, although inadmissible when conducting a tension test using a directionally homogeneous test coupon such as, for example, a flat layered system loaded in one of its principal orthotropic directions, it has been consistently observed by researchers testing woven composite coupons. In the absence of rigorous mechanical models, several hypotheses aiming at justifying the above microstrain surface measurements have been developed. A leading hypothesis is that the surface microstrains are obtained as a result of local micro-bending induced during bundle stretching. In order to assist in the clarification of the above issue, microstrain and microstress contours obtained using the 3-D finite element single woven ply *soft*-matrix model are shown in Figures 12 and 14 and results for the *stiff*-matrix model are shown in Figures 15–17. For consistency purposes, it is also important to mention that the microstrain and microstress results shown in Figures 12–17, correspond to a bundle height aspect ratio of $b/a = 0.2$. Other specific model parameters are given in Tables 1 and 3 for the *soft*- and *stiff*-matrix

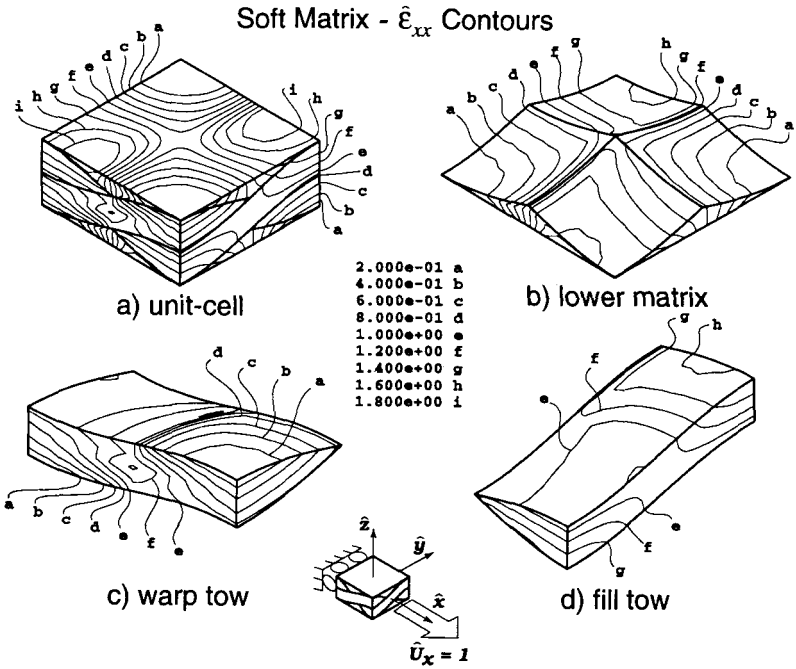

Figure 12. *Contour plots of the normalized microstrain $\hat{\varepsilon}_{xx}$ relative to the global coordinate system.*

models, respectively. The strain results are normalized with the characteristic strain $\varepsilon_c = U_x/a$ where U_x is the applied axial displacement. The stress results are normalized with the characteristic stress $\sigma_c = \varepsilon_c E_c = U_x E_f/a$.

Contours of the component of strain in the global x direction are shown in Figures 12 and 15 for the *soft*- and *stiff*-matrix systems respectively. These results illustrate two different patterns of micro-bending. In the case of the *soft*-matrix composite shown in Figure 12, strong micro-bending is observed normal to the fill tow centroidal axis and to a lesser extent transverse to the warp tow centroidal axis. In the case of the *stiff*-matrix woven unit-cell shown in Figure 15, micro-bending is observed transverse to the warp tow centroidal axis and normal to the centroidal axis of the fill tow near the mid-section. In each case it is noted that the micro-bending strains are transferred through the interbundle matrix. We also note that in CVI ceramic systems, the length of the unit-cell l may often be on the order of 1–3 mm. As such the micro-bending phenomenon may be detected experimentally by placing sufficiently small strain gauges in the regions of elevated strain as predicted by the finite element results.

Each of the normal stress components relative to the local material coordi-

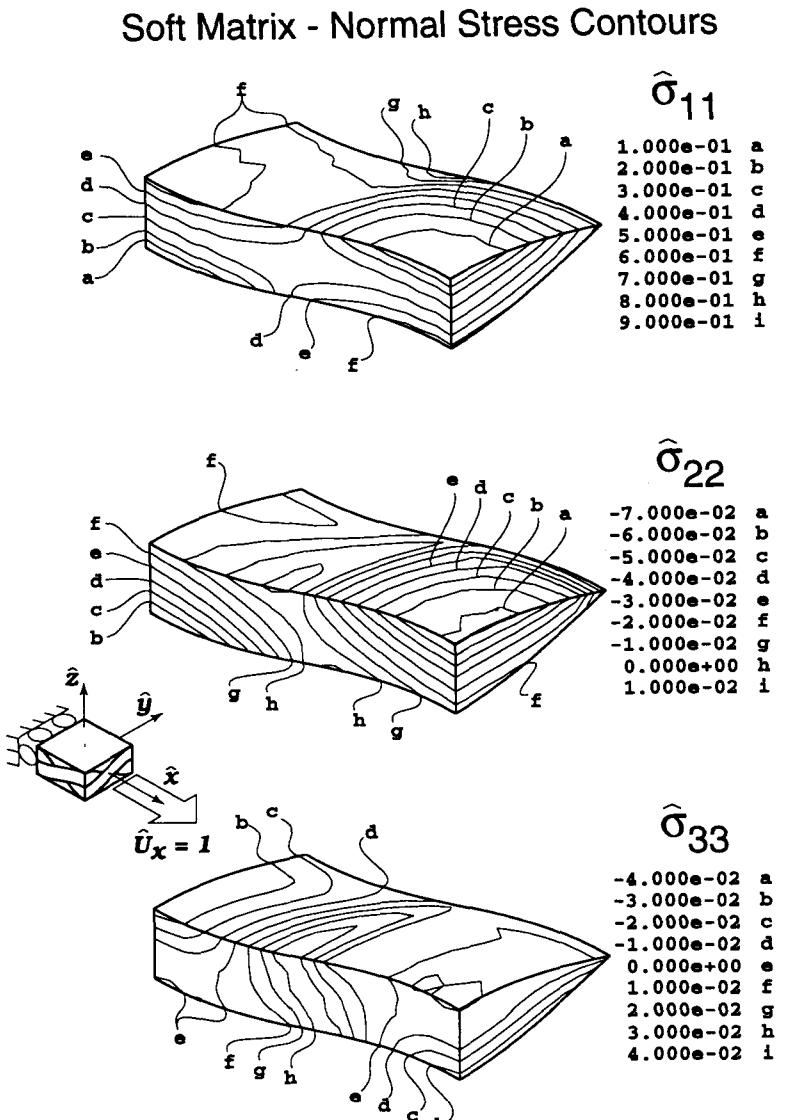

Figure 13. *Warp bundle surface contour plots of the non-dimensional shear stresses expressed with respect to the local system (1,2,3) aligned with the spatially varying local principal material directions consistent with the model formulation presented in Part I.*

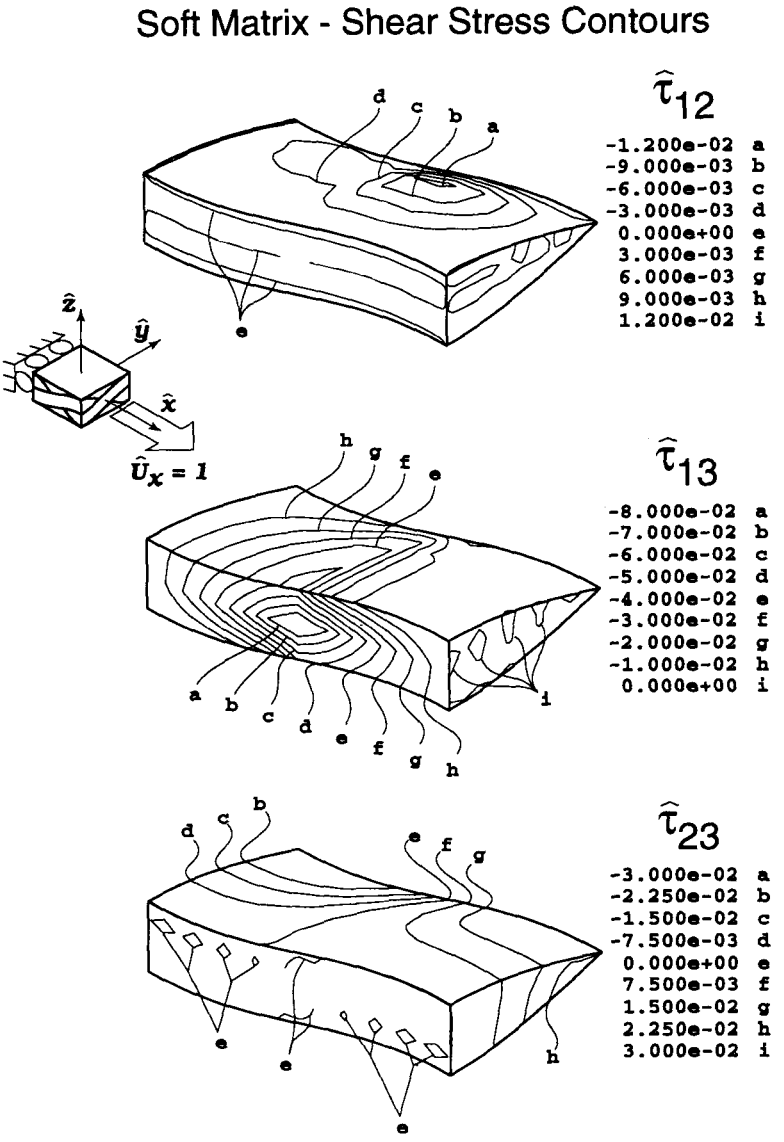

Figure 14. *Warp bundle surface contour plots of the non-dimensional shear stresses expressed with respect to the local system (1,2,3) aligned with the spatially varying local principal material directions. The results correspond with the results presented in Figure 13.*

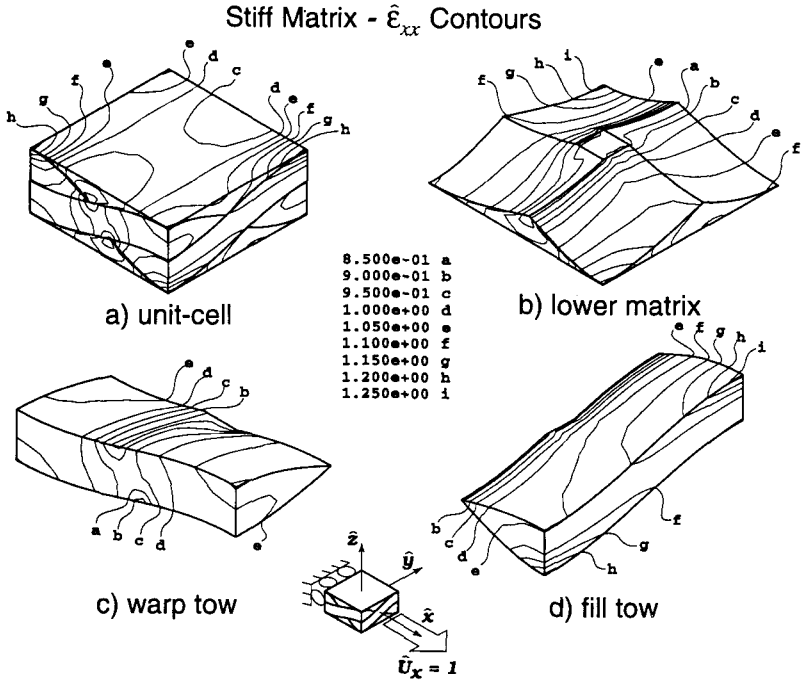

Figure 15. *Contour plots of the normalized microstrain $\hat{\varepsilon}_{xx}$ relative to the global coordinate system.*

nate system are displayed on the surfaces of the fill tow in Figures 13 and 16 for the *soft-* and *stiff-*matrix woven composites, respectively. Micro-bending is again illustrated in the contour plots of the σ_{11} components. The corresponding shear stress components are shown in Figures 13 and 16. We note that the out-of-plane shear and normal stress components are roughly an order of magnitude less than those in the loading direction. The modified lamination theory presented earlier is based on an assumption of plane stress, and while we observe that out-of-plane stresses do exist, the assumption appears to be a good approximation. These components of stress, while relatively small, may play an important role in the development of damage such as delamination. Also note the existence of regions of stress concentrations in Figures 13 and 16 which may give rise to microdamage during the early stages of loading of the woven systems. Such evidence suggest that the overall effective response of CVI ceramic matrix woven systems may exhibit appreciable nonlinearities early on in their loading history as a result of the stress-driven damage evolution.

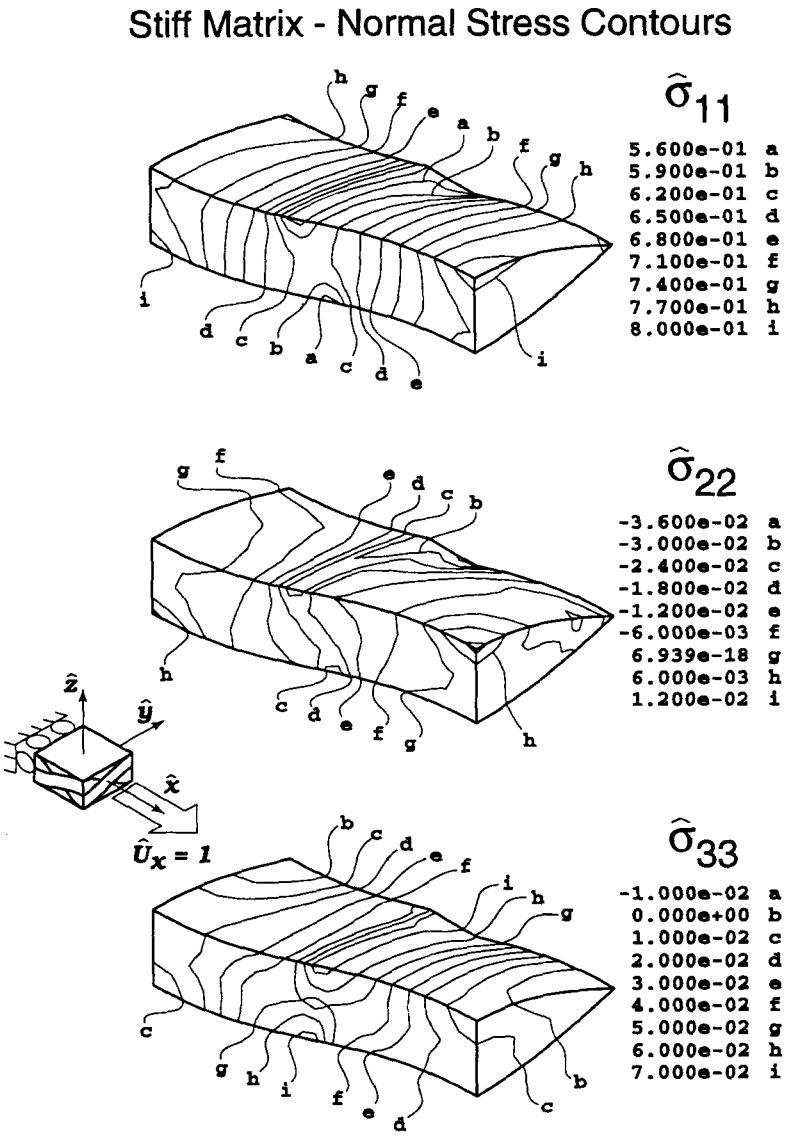

Figure 16. *Warp bundle surface contour plots of the non-dimensional normal stresses expressed with respect to the local system (1,2,3) aligned with the spatially varying local principal material directions.*

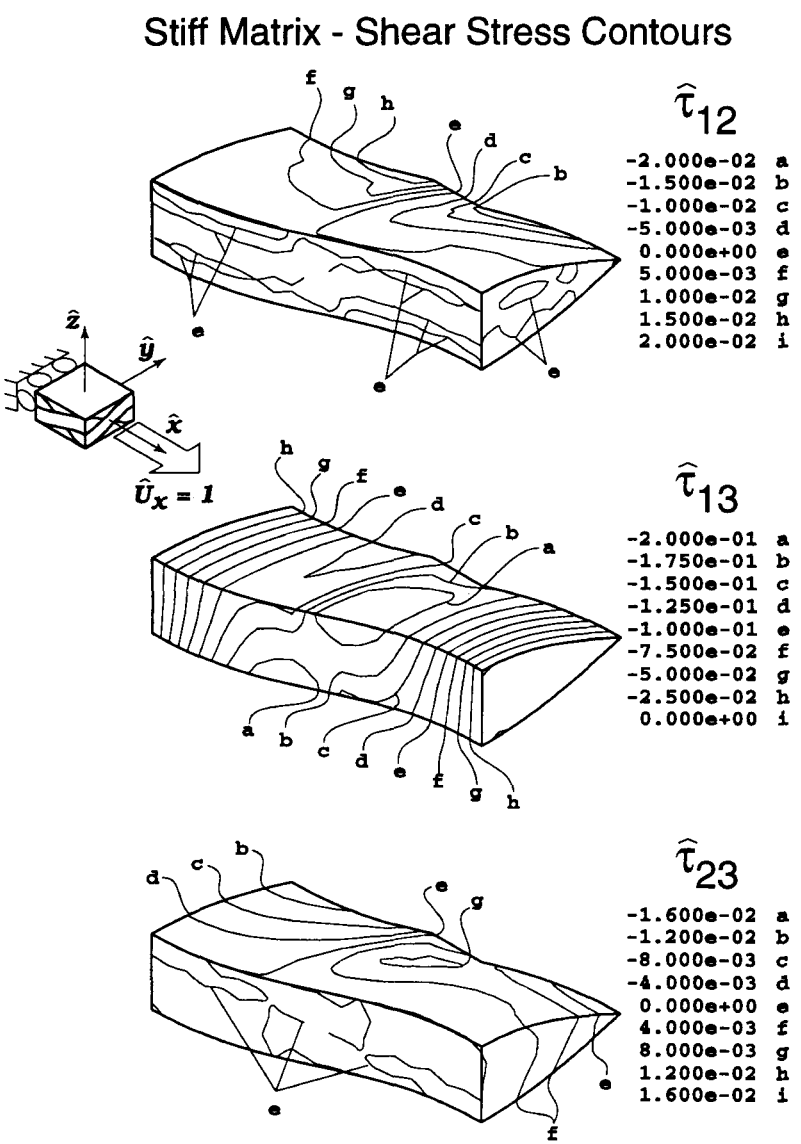

Figure 17. *Warp bundle surface contour plots of the non-dimensional shear stresses expressed with respect to the local system (1,2,3) aligned with the spatially varying local principal material directions. The results correspond with the normal stresses reported in Figure 16.*

CONCLUSIONS

Extensive parameter studies, have shown that the Parallel (P-MLT) averaging model predictions are in closer agreement with the 3-D finite element results for both the *soft*- and *stiff*-matrix woven systems. The above studies, have shown that the effects of microporosity either within the bundle or within the interbundle matrix, as well as the concurrent or independent presence of relatively soft fiber and bundle coatings may significantly reduce the effective elastic properties of the composite. *Soft*-matrix systems such as polymer woven composites, were also shown to exhibit a greater sensitivity to the effects of unit-cell geometry as compared to the response of *stiff*-matrix systems such as the CVI ceramic matrix woven composites. In addition, single and multiple woven symmetric layer finite element studies suggest that the analytical MLT models substantially underestimate the in-plane effective elastic properties of *soft*-matrix single woven layer systems. At the same time the analytical models, were shown to be in excellent agreement with the 3-D finite element results for *soft*-matrix multiple layer laminates as well as for both single and multiple layer *stiff*-matrix woven systems. The models which were developed in a companion study (Part I), can be used to interpret related experimental data obtained using either *soft*-polymer matrix or *stiff*-ceramic woven composites aiming at establishing the elastic response of woven systems comprised of relatively complex microstructures.

Microstress and microstrain finite element results suggest that the interior of woven composites is subjected to a highly triaxial state of stress. High stress concentration was shown to dominate the near vicinity regions of the inner bundle/interbundle matrix interface. Pronounced micro-bending induced during stretching by the undulating bundles was also observed. These results, further highlight the need for the development of non-linear models capable of predicting the effective response of woven systems undergoing local microdamage that would most likely evolve under the highly triaxial state of stress dominating the interior of such woven systems even when macroscopically loaded in either pure tension or shear.

ACKNOWLEDGEMENTS

Support for this work was provided by the National Science Foundation, Grant No. CMS94-96209. Discussions with Professors Frank Zok and Rajendra Bordia are readily acknowledged.

REFERENCES

1. J. L. Kuhn and P. G. Charalambides. 1996. "Elastic Response of Porous Matrix Plain Weave Fabric Composites: Part I—Modeling." *J. Composite Mater.*, 32(16):1472–1506.

2. Frank Zok, John McNulty, and Todd Steyer. Private Communication. Materials Department, University of California, Santa Barbara.
3. T. E. Steyer and F. W. Zok. 1996. "Stress Rupture of An SiC/SiC Composite." Presented at *The American Ceramic Society 1996 Annual Meeting & Exposition,* Indianapolis, Ind.
4. J. C. McNulty and F. W. Zok. 1996. "Notch Sensitivity of SiC/SiC at Ambient and Elevated Temperatures." Presented at *The American Ceramic Society 1996 Annual Meeting & Exposition,* Indianapolis, Ind.
5. Rajendra K. Bordia, David H. Roach, and Samuel M. Salamone. 1995. "Crack Growth Resistance of CVI Processed Ceramic Matrix Composites." *Proceedings of ICCM.*
6. Rajendra K. Bordia, David H. Roach, and Samuel M. Salamone, and Mark Headinger. "Tensile Properties and Crack Growth Resistance of Ceramic Matrix Composites." *Submitted for publication to the J. Amer. Ceram. Soc.*
7. Takashi Ishikawa and Tsu-Wei Chou. 1982. "Elastic Behavior of Woven Hybrid Composites." *J. Composite Mater.,* 16:2–19.
8. T. Ishikawa and T. W. Chou. 1982. "Stiffness and Strength Behaviour of Woven Fabric Composites." *J. Mater. Sci.,* 17:3211–3220.
9. Takashi Ishikawa and Tsu-Wei Chou. 1983. "In-Plane Thermal Expansion and Thermal Bending Coefficients of Fabric Composites." *J. Composite Mater.,* 17:92–104.
10. Takashi Ishikawa and Tsu-Wei Chou. 1983. "One-Dimensional Micromechanical Analysis of Woven Fabric Composites." *AIAA J.,* 21(12):1714–1721.
11. Tsu-Wei Chou and Takashi Ishikawa. 1989. "Analysis and Modeling of Two-Dimensional Fabric Composites." In Tsu-Wei Chou and Frank K. Ko, editors, *Textile Structural Composites: Composite Materials Series,* volume 3, pp. 209–264. Elsevier Science Publishers B. V.
12. Takashi Ishikawa, Masamichi Matsushima, Youichi Hayashi, and Tsu-Wei Chou. 1985. "Experimental Confirmation of the Theory of Elastic Moduli of Fabric Composites." *J. Composite Mater.,* 19:443–458.
13. N. K. Naik and P. S. Shembekar. 1992. "Elastic Behavior of Woven Fabric Composites: I-Lamina Analysis." *J. Composite Mater.,* 26(15):2196–2225.
14. N. K. Naik and V. K. Ganesh. 1992. "Prediction of On-Axes Elastic Properties of Plain Weave Fabric Composites." *Composites Sci. & Tech.,* 45:135–152.
15. Ivatury S. Raju and John T. Wang. 1994. "Classical Laminate Theory Models for Woven Fabric Composites." *J. Composite Tech. & Res.,* 16(4):289–303.
16. S. Shkoller and G. Hegemier. 1995. "Homogenization of Plain Weave Composite Using Two-Scale Convergence." *I. J. Sol. & Struc.,* 32(6–7):783–794.
17. A. Dasgupta and S. M. Bhandarkar. 1994. "Effective Thermomechanical Behavior of Plain-Weave Fabric-Reinforced Composites Using Homogenization Theory." *J. Engr. Mater. & Tech.,* 116:99–105.
18. Y. C. Zhang and J. Harding. 1990. "A Numerical Micromechanics Analysis of the Mechanical Properties of a Plain Weave Composite." *Computers and Structures,* 36(5):839–844.
19. John D. Whitcomb. 1991. "Three-Dimensional Stress Analysis of Plain Weave Composites." In T. K. O'Brien, editor, *Composite Materials: Fatigue and Fracture (Third Volume), ASTM STP 1110,* pp. 417–438. American Society for Testing and Materials, Philadelphia.
20. K. Ranji Vaidyanathan, Ajit D. Kelkar, and Jagannathan Sankar. 1993. "Prediction of Elastic Properties of Ceramic Matrix Composites Using a Plain Weave Classical Laminate Theory." *Ceram. Engr. Sci. Proc.,* 14(9–10):1066–1076.
21. Wen-Shyong Kuo and Tsu-Wei Chou. 1995. "Elastic Response and Effect of Transverse Cracking in Woven Fabric Brittle Matrix Composites." *J. Amer. Ceram. Soc.,* 78(3):783–792.
22. John L. Bassani. 1991. "Linear Densification and Microcracking in Sintering Compacts." In *Mech. of Mater.,* volume 12, pp. 119–130. Elsevier Science Publishers B. V.
23. J. L. Kuhn and P. G. Charalambides. 1997. "Elastic Micro-Fields in Plain Weave Fabric Composites under Remote In-Plane Loading." *In Progress.*